

Stress Evolution of Rock-Like Specimens Containing a Single Fracture Under Uniaxial Loading: a Numerical Study Based on Particle Flow Code

Jie Liu · Jun Wang

Received: 2 April 2017 / Accepted: 18 August 2017 / Published online: 22 August 2017
© Springer International Publishing AG 2017

Abstract Stress concentrations are responsible for the crack propagation in rock and rock-like specimens. To investigate the stress evolution characteristics of the rock-like specimens containing a single prefabricated fracture, a numerical study based on the particle flow code was conducted. The numerical results indicate that the concentrated tensile stress and shear stress are responsible for the wing and secondary crack propagation. At the early compression stage, wing cracks tend to form by the concentrated tensile stress, whereas the secondary crack forms by the shear plane resulting from the shear stress concentration at later compression stage. Additionally, the increase in the inclination angle restrains the wing crack propagation. Moreover, in the propagation process of the typical wing and secondary cracks, sudden decreases of the tensile and shear stresses are observed. These decreases at the former monitor points are always accompanied with the sharp increases at the latter points. Furthermore, the results show that the wing and secondary cracks develop in different manners. The large axial strain gaps between adjacent monitor points for wing crack propagation indicates that the

wing crack propagates in a stable and slow way, whereas the significantly reduced gaps indicate that the secondary crack propagates in a speedy and unstable way.

Keywords Stress evolution · Rock-like specimen · Single fracture · Particle flow code

1 Introduction

Small open fractures, which may decrease the mechanical properties of rock mass, are common in rock mass (Fig. 1). Cracks, which initiate from the tips of these fractures under external loading, may further determine rock failure characteristics and affect the rock mass stability. Thus, aiming to improve the stability of the rock mass that contains small fractures, extensive studies have been conducted to investigate the crack initiation, propagation and coalescence mechanism in rock and rock-like specimens (Wang and Cao 2017; Duriez et al. 2016; Fan et al. 2015; Gratchev et al. 2016). For the crack initiation at the tips of small fractures, first, according to the various crack initiation and propagation modes that are shear and tensile modes, Wong and Einstein proposed seven types of cracks (Wong and Einstein 2009). Second, because of the variation of initiation sequence, two types of cracks, which are wing cracks and secondary cracks, have been proposed (Bobet and Einstein 1998).

J. Liu (✉) · J. Wang
Department of Building Engineering, Hunan Institute of Engineering, Xiangtan, China
e-mail: ljydsj@163.com

J. Liu
Hunan Provincial Key Laboratory of Safe Mining
Techniques of Coal Mines, Xiangtan, China

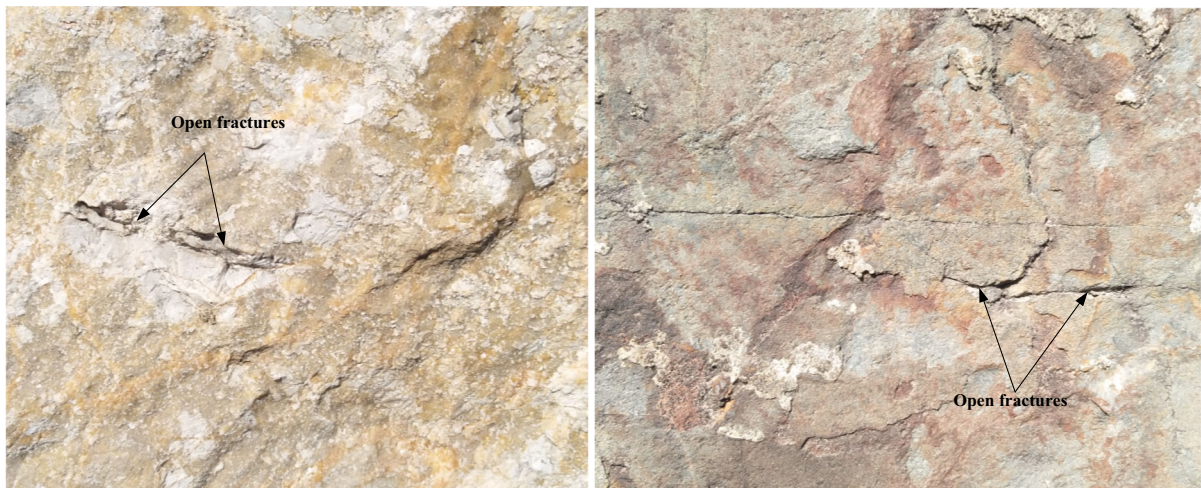


Fig. 1 Open fractures in the rock

Wing cracks first initiate from or near the tips of small fractures and subsequently propagate along the maximum compression trajectory. Then, secondary cracks, which may result from the shear, tensile or shear-tensile force concentration, initiate from the tips and propagate in various directions. By analyzing the stress conditions at the wing, shear and anti crack segments, numerical study by Gonçalves da Silva obtained similar results (Gonçalves da Silva and Einstein 2013). In addition, Zhou proposed five types of cracks based on the differences in the initiation sequence, location and mode (Zhou et al. 2013). Simultaneously, some other crack classifications have also been reported (Huang et al. 2015; Zhang et al. 2016).

After crack initiation, coalescence, which significantly determines the failure characteristics and mechanical properties of rock specimens, occurs by the crack propagation. To comprehensively investigate the coalescence mechanism, extensive experimental and numerical studies instead of the difficult field study have been conducted. First, Cao's laboratory tests proposed seven coalescence patterns of the specimens containing two small fractures (Cao et al. 2015). The laboratory investigation by Zhao indicated that tensile cracks are more favorable for a larger rock bridge ligament angle (Zhao et al. 2016). Haeri's laboratory tests indicated that the coalescence is affected by the length and orientation of the prefabricated fractures (Haeri et al. 2014). In additions, Zhang's numerical study

proposed eleven crack coalescence types that are determined by the fracture inclination angle, ligament length, and bridging angle (Zhang et al. 2015). Camones applied the 3D Particle Flow Code to analyze the step-path failure mechanism of a slope, and he proposed that the coalescence results from the connection of the secondary coplanar cracks (Camones et al. 2013).

In previous studies, the effect of initial fracture and rock bridge characteristics on the crack initiation, propagation and coalescence mechanisms have been comprehensively investigated. However, limited studies have been conducted on the impetuses, the concentrated stresses, which dominate crack initiation and propagation using discrete method. Recent, the numerical study by Xie studied the stress condition at tips of the single prefabricated fracture under uniaxial compression (Xie et al. 2016). The initiation and propagation of wing cracks were properly studied, however, the propagation of the secondary cracks was not discussed. In addition, the effect of the prefabricated crack on the stress conditions near tips has not been properly investigated using discrete element method.

Thus, in the present article, to study the evolution of the tensile and shear stress concentrations, driving the crack propagation, a numerical study based on the 2D particle flow code (PFC 2D) was conducted. The influence of the inclination angle and axial strain on the crack propagation was investigated by analyzing the concentrated stresses. Then, the propagation

patterns of typical wing and secondary cracks were discussed.

2 Numerical Tests

In the present article, the 2D particle flow code (PFC 2D), which is a commonly used DEM code, was applied to investigate the crack initiation, propagation and coalescence in the specimens containing prefabricated fractures. As shown in Fig. 2a, the intact model, whose width and height were 0.15 and 0.2 m, consisted of 53,920 particles. The radius of the particles ranged from 0.24 to 0.40 mm. After the generation of the particles, an isotropic stress of 1 MPa, defined as the mean of the direct stresses, was achieved. Parallel bonds can resist shear, tensile and bending between particles, thus, parallel bonds can properly simulate the micro behavior of soil and rock (Cao et al. 2016a). Therefore, 136,152 parallel bonds instead of contact bonds were installed between particles. Micro cracks form between particles when the normal and shear stress reach their normal and/or shear strength. Detailed micro parameters of particles and parallel bonds are listed in Table 1. To make numerical results comparable to laboratory results reported by Jin’s study where the uniaxial compressive strength of the specimen is 27.26 MPa (Jin et al. 2017), the calibration process shown in Fig. 2b was conducted by performing the uniaxial compression test on the intact specimen that has been proven a validate calibration method (Cao et al. 2016b), and the

macro parameters of this synthetic material are listed in Table 1. The calibrated uniaxial compressive stress equaling to 26.5 MPa indicates that the numerical model of the intact specimen is reasonable.

The prefabricated fracture, as shown in Fig. 3, can be generated by deleting particles at the specific locations. To investigate the influence of the inclination angle, β , on crack initiation and propagation, six prefabricated fractures with a length of 2 cm and six inclination angles, which were 0°, 15°, 30°, 45°, 60° and 75°, were generated in six specimens. Before loading, 7500 measure circles with a radius of 1 mm were installed in the test model to monitor the stresses. According to the logic of measure circles (Itasca 2002), the average stresses in the X, Y and X–Y direction can be calculated and restored. In PFC 2D, the tensile and compression stresses are positive and negative, respectively. Thus, according to the recent study by Xie (Xie et al. 2016), the tensile stress, which is the positive maximum principle stress, can be viewed an effective indicator for wing crack propagation:

$$\sigma_{\max} = \frac{\sigma_h + \sigma_v}{2} + \sqrt{\left(\frac{\sigma_h - \sigma_v}{2}\right)^2 + \tau^2}$$

where σ_{\max} is the maximum principle stress; σ_h and σ_v are the horizontal and vertical stress; τ is the shear stress.

In the loading process, the axial compression was applied by moving the upper wall with a constant rate of 0.5 mm/min with the lateral surfaces unconfined. The stresses in measure circles were recorded every 200 steps.

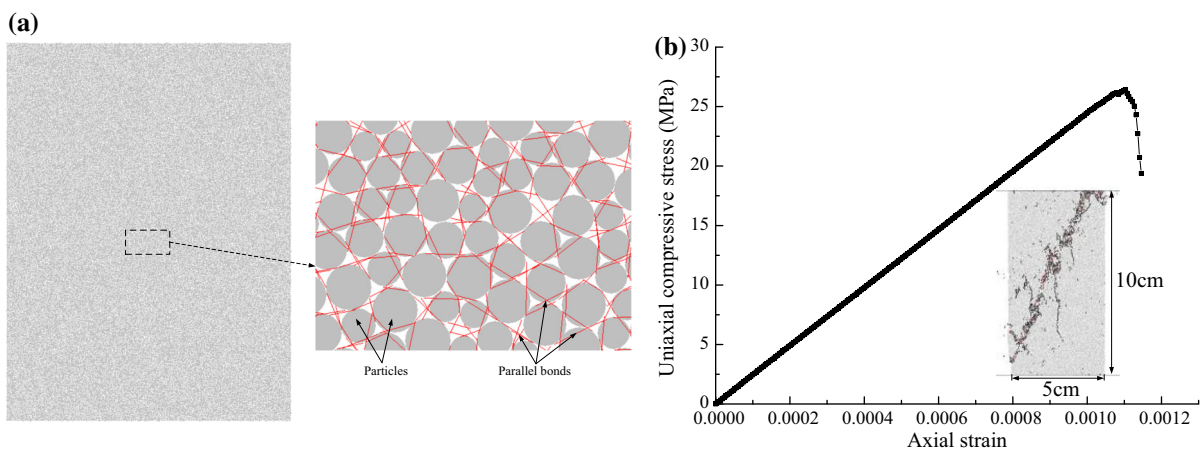
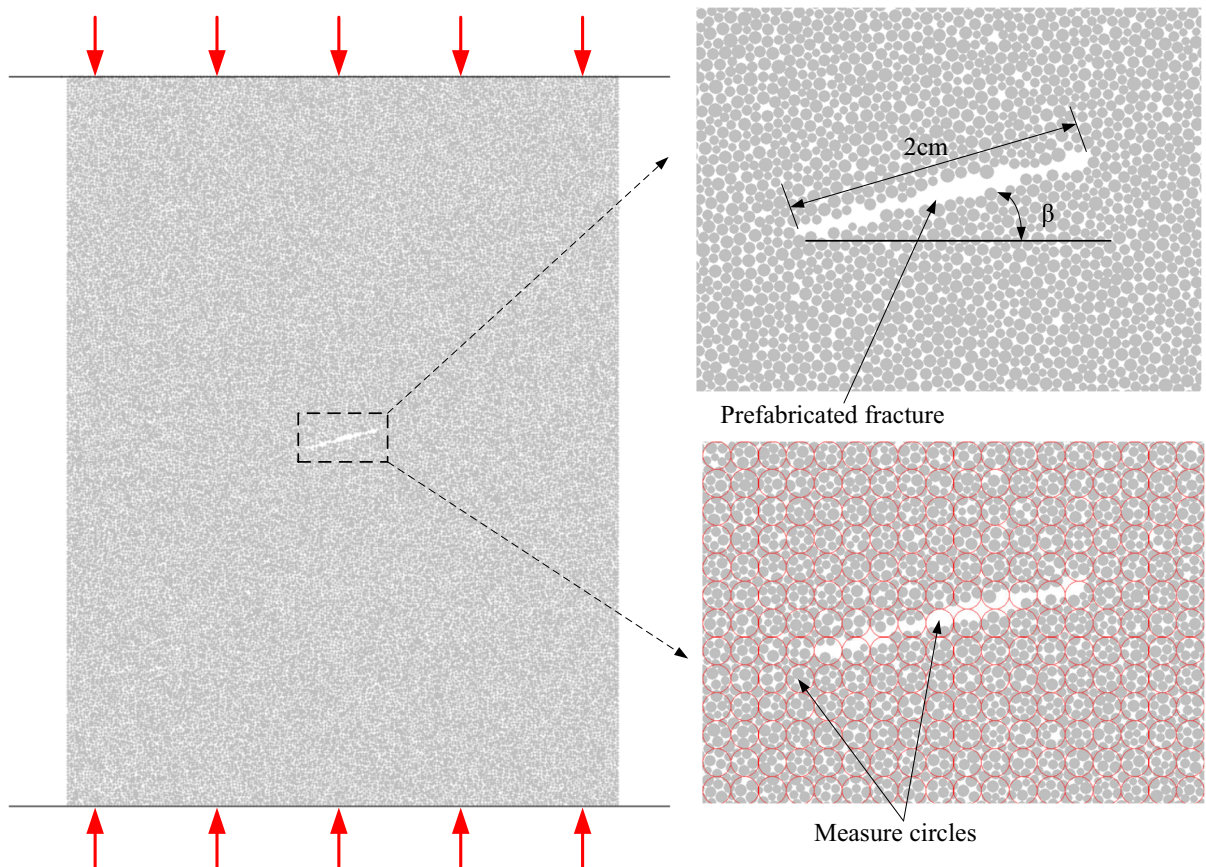


Fig. 2 The intact numerical model and the calibration of the uniaxial compressive strength **a**: the intact model; **b** the calibration model

Table 1 Micro and macro synthetic parameters

Micro-parameters	Values	Macro parameters	Value
Minimum radius (mm)	0.24	Uniaxial compression stress, UCS (MPa)	26.5
R_{\max}/R_{\min}	1.66		
Particle contact modulus (GPa)	9.5		
Particle normal/shear stiffness	2.5	Young's modulus, E (GPa)	2.4
Friction coefficient	0.5		
Parallel bond modulus (GPa)	1.95		
Parallel normal/shear stiffness	2.5	Poisson ratio	0.22
Parallel bond normal strength (MPa)	17.9		
Parallel bond shear strength (MPa)	17.9		

**Fig. 3** Numerical test model and *measure circles*

3 Results and Discussion

3.1 Comparison on Crack Initiation Between Laboratory and Numerical Studies

Figure 4 shows the laboratory sketch pictures for the crack initiation in Jin’s study and the numerical results in the present numerical study (Jin et al. 2017). The specifications of the present numerical model, including the crack length and inclination angles, are the same to those in Jin’s study. Thus, the present

numerical models can properly simulate the laboratory tests by Jin. When the inclination angle, β , is 0° , a wing crack initiates from the right tip, whereas a wing crack initiates at a location that deviates from the left tip. When β increases to 15° , a similar wing crack initiates from the right tip. Simultaneously, the distance between the initiation point of the left wing crack and the left tip of the prefabricated fracture slightly decreases. With further increase in the inclination angle, wing cracks and secondary cracks initiate from the tips. When the inclination angle

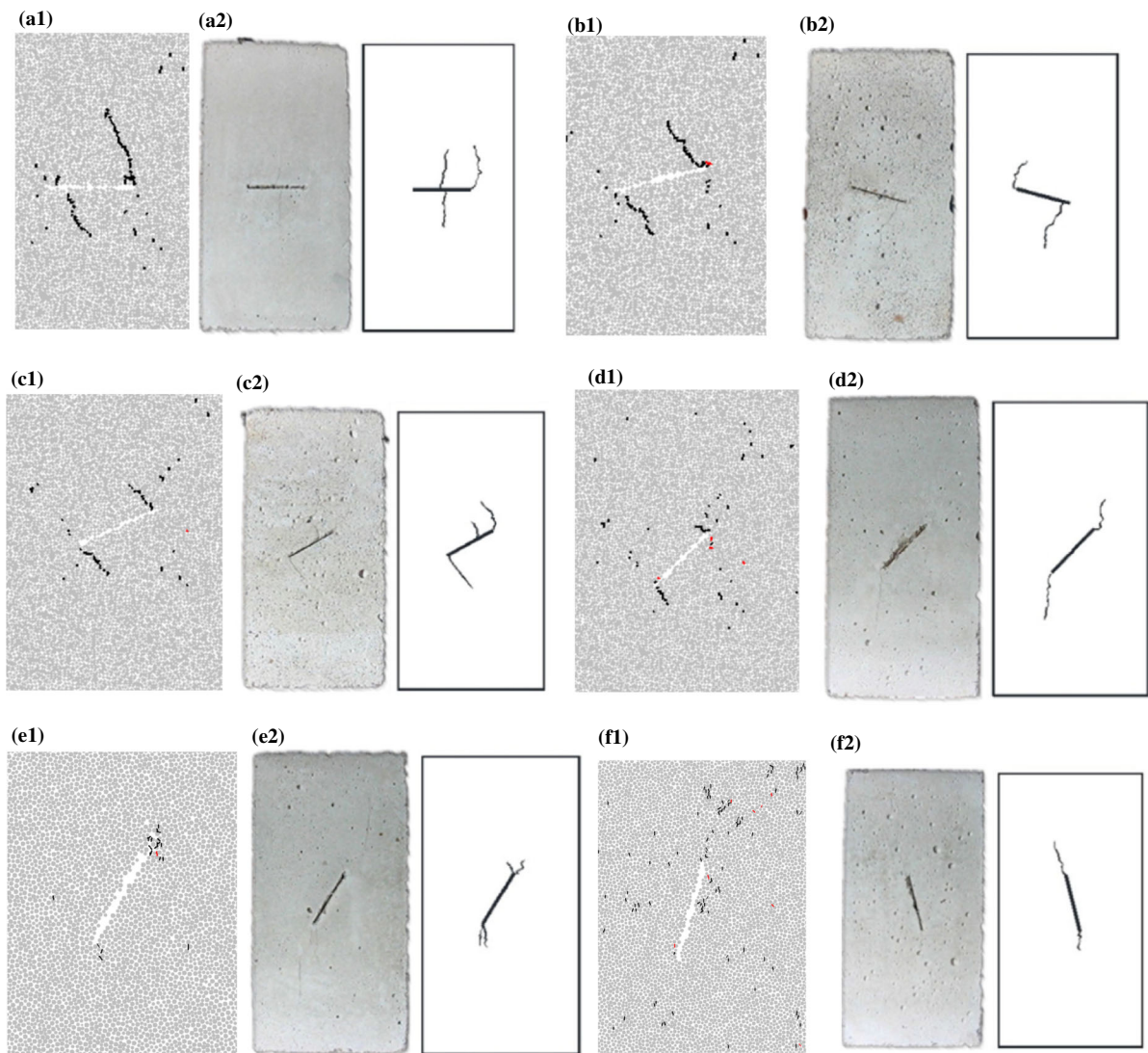


Fig. 4 Crack initiations for various inclination angles in laboratory and numerical tests: **a1–f1** are the numerical results; **a2–f2** are the laboratory results

increases to 60° and 75° , only shear cracks form under compression. In Jin's study, the displacement of the particles was successfully and vividly used to characterize the crack propagation. However, the evolution of the stresses driving the movement of the particles remains unclear during the crack propagation process. Thus, following study mainly focuses on the stress evolution on crack propagation.

3.2 Stress Evolution in the Compression Process

The stress evolution for various axial strains is depicted in Fig. 5 when the inclination angle is 0° . A tensile stress concentration zone, where the maximum tensile stress is about 3 MPa (Fig. 5), forms when the axial strain is 0.1%. Simultaneously, three shear stress concentration zones, where the maximum shear stress

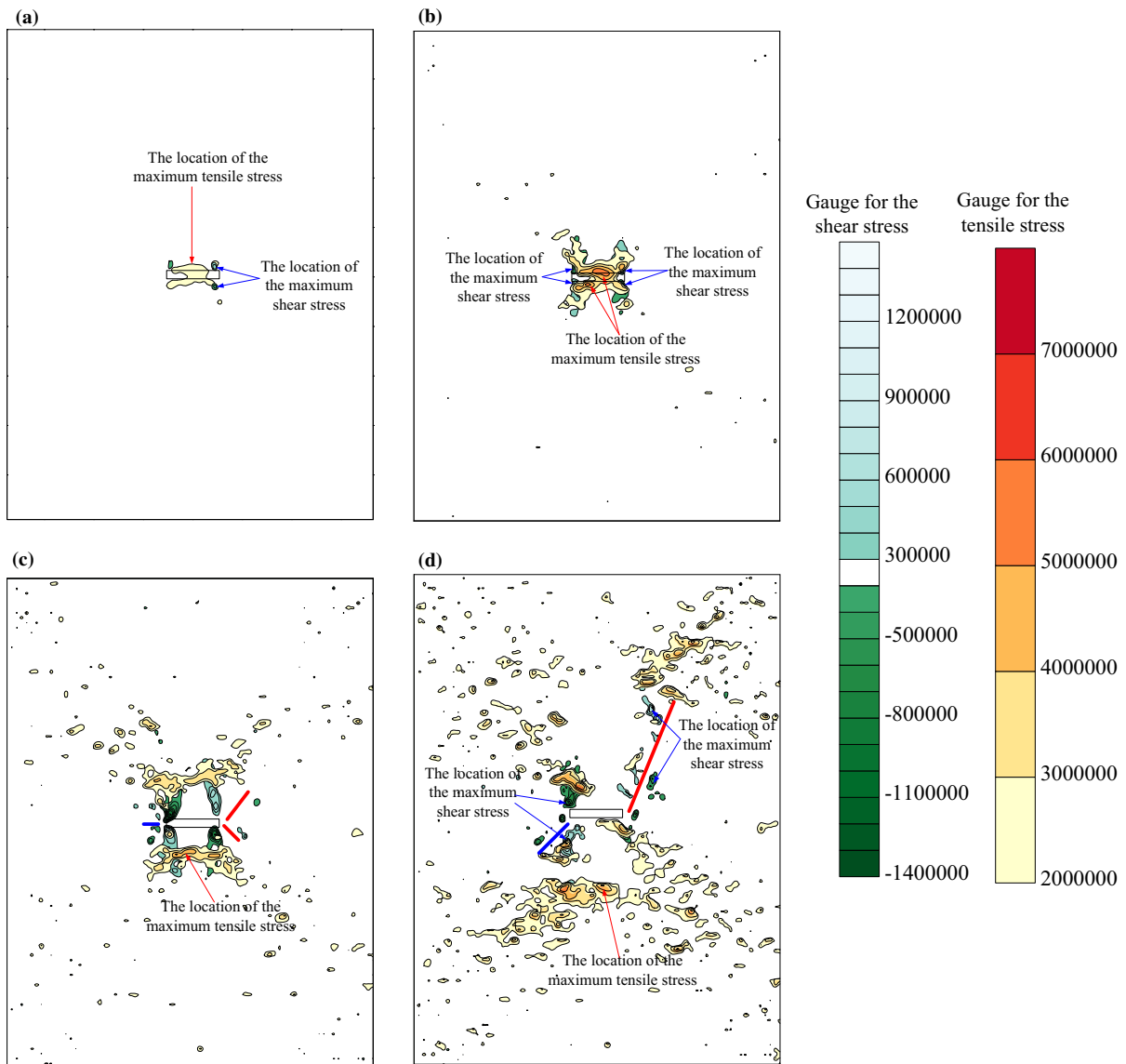


Fig. 5 Stress evolution for various axial strain when the inclination angle is 0° : **a–d** are the stress conditions when the axial strains are 0.1, 0.2, 0.3 and 0.4%

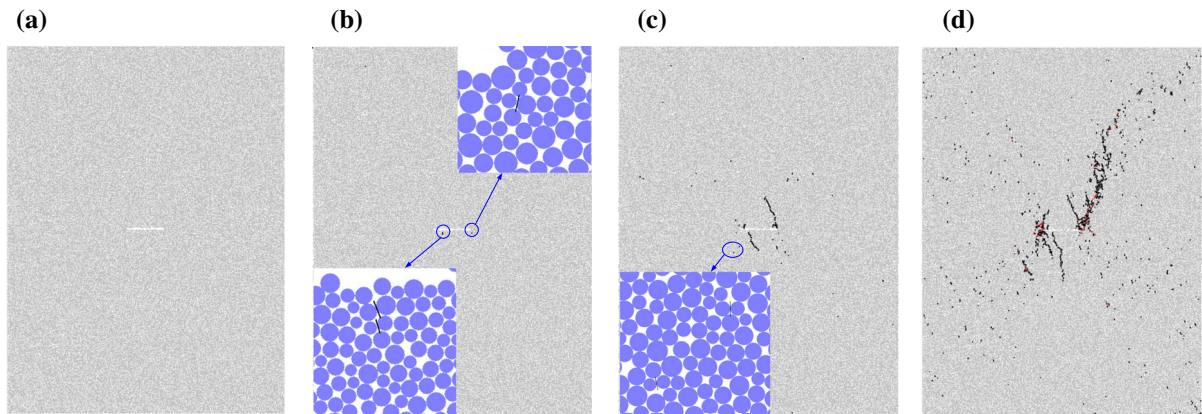


Fig. 6 Crack initiation and propagation for various axial strains: **a–d** are the crack propagation when the axial strains are 0.1, 0.2, 0.3 and 0.4%

was only 3.7 MPa, are formed at the tips. The intact specimen in Fig. 6a indicates that no micro crack forms. In other words, the concentrated tensile and shear stresses cannot cause bond breakages at the axial strain of 0.1%. When the axial strain increases to 0.2%, the tensile stress concentration zones, where the maximum tensile stress increases to 5.6 MPa, develop on the two sides of the prefabricated fracture. With the micro cracks in Fig. 6b, a wing crack forms at the location that deviates from the left tip. Simultaneously, the shear stress concentration zones are enlarged. The maximum shear stress increases to 6.4 MPa that cannot cause shear breakages (Fig. 6b). With further increase of axial strain to 0.3%, the location of the maximum tensile stress further propagates in the direction the compression stress acts. However, the maximum tensile stress slightly decreases to 5.1 MPa. This decrease in the tensile stress may result from the wing crack propagation (Fig. 6c), and the maximum shear stress further increases to 9.2 MPa. The concentrated shear stresses indicate that a shear plane, which is denoted by a blue line, forms at the left tip where the concentrated shear stresses act in the opposite directions. Simultaneously, two shear planes denoted by red lines are formed at the right tip. With the further axial strain increase to 0.4%, the location of the maximum tensile stress, which is 5.9 MPa, overlaps with the left wing crack tip and the shear stress concentration zones in Fig. 6d. The shear planes, where the maximum shear stress slightly decreases to 9.0 MPa, significantly develop at the

tips. These developments of the shear planes may be responsible for the propagation of the secondary cracks at the tips of the prefabricated fracture in Fig. 6d.

When the inclination angle increases to 30°, two independent tensile concentrated zones with diminished areas form at the tips for an axial strain of 0.1%. Simultaneously, the shear concentration zones also shrink. When the axial strain increases to 0.2%, the tensile and shear concentration zones significantly develop. During the develop process, two wing cracks, whose tips overlap with the tensile concentration zones, initiate and propagate at the tips. With a further axial strain increase to 0.3%, two shear plane denoted by red lines at the right tip and another shear plane denoted by a blue line at the left tip form (Fig. 7). The tensile concentration zones significantly develop and overlap with the shear concentration zones. The location of the maximum tensile stress slightly moves away from the location when the axial strain is 0.2%, this slight movement might be responsible for the slight propagation of the wing cracks (Fig. 8b, c). When the axial strain further increases to 0.4%, the shear planes, which are responsible for the shear failure in Fig. 8d, significantly develop. However, the tensile concentration for wing crack propagation continues to dissipate.

When the inclination angle further increases to 60°, the concentrated tensile and shear stresses are lower than 2 and 3 MPa for an axial strain of 0.1%, respectively. Thus, the corresponding stress

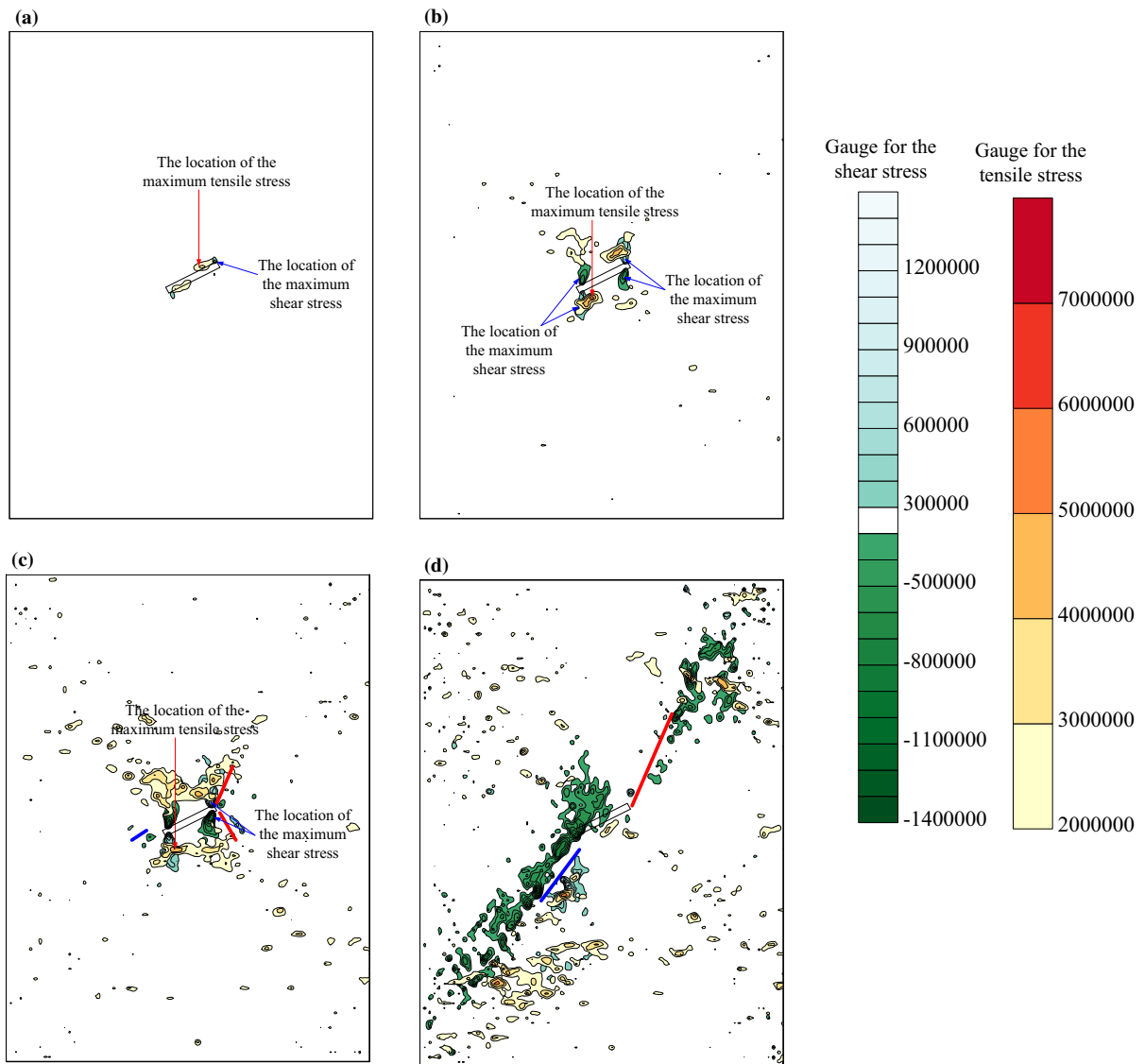


Fig. 7 Stress evolution for various axial strain when the inclination angle is 30° : **a–d** are the stress conditions when the axial strains are 0.1, 0.2, 0.3 and 0.4%

conditions are not involved in Fig. 9. When the axial strain is 0.2%, tensile and shear concentration zones, which are much smaller than those in Fig. 7, overlap at the tips of the prefabricated fissure. With the increase of axial strain, similar developments of the tensile and shear concentration zones and the formation of the shear plane are observed. The restrained developments of tensile and shear concentration result in the restrained crack initiation and propagation in Fig. 10.

To further investigate the stress evolution in the compression tests, the maximum tensile and shear

stresses for various axial strains are depicted in Fig. 11. Figure 11 shows that the maximum tensile stress first increases with the increase of the axial strain when the inclination angle is lower than 30° . Then, a subsequent decrease followed by an increase is observed with the further increase in axial strain. These increases and decrease can be demonstrated by the propagation of wing and secondary cracks. As shown in Figs. 7a, the maximum tensile stress locations locate at the tips of the prefabricated fissure. Because of the relatively low tensile stress in Fig. 11a,

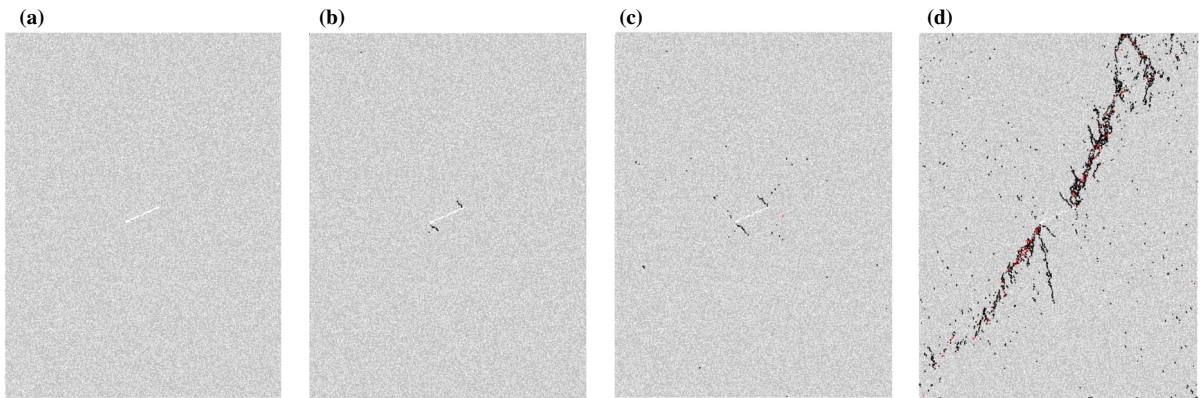


Fig. 8 Crack initiation and propagation for various axial strains: **a–d** are the crack propagation when the axial strains are 0.1, 0.2, 0.3 and 0.4%

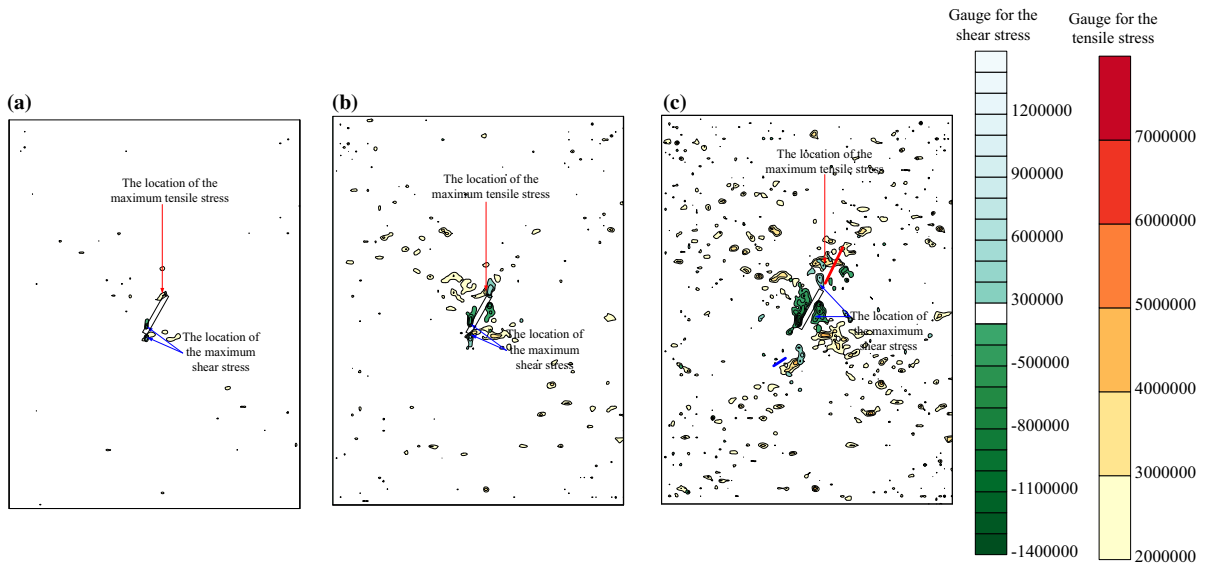


Fig. 9 Stress evolution for various axial strain when the inclination angle is 60°: **a–c** are the stress conditions when the axial strains are 0.2, 0.3 and 0.4%

no wing crack forms when the axial strain is 0.1% (Fig. 8a). When the axial strain increases to 0.2%, the tensile stress concentration zones, which overlap with the wing crack tips, enlarge, and simultaneously, the increased tensile stress is high enough to cause the wing crack propagation (Fig. 8b). When the wing crack further propagates, the tensile stress concentration at the wing crack tips dissipates, resulting in the decrease of the maximum tensile stress when the axial strain is 0.3%. When the axial strain further increases, stress concentrations, which will cause the initiation and propagation of secondary cracks, proceed and result in the second increase of the tensile stress.

When the inclination angle is 60° and 75°, the maximum tensile stress increases with the increase in the axial strain. This phenomenon may result from the fact that no wing crack forms in the compression process (Fig. 4e1, f1). Thus, the locations of the maximum tensile stress overlap with the shear concentration zones (Fig. 9). The stress concentrations before the secondary crack propagation will result in these increases of the maximum tensile stresses.

Figure 11b shows that the maximum shear stress increases with the increase in the axial strain. Figures 6, 8 and 10 indicate that secondary cracks

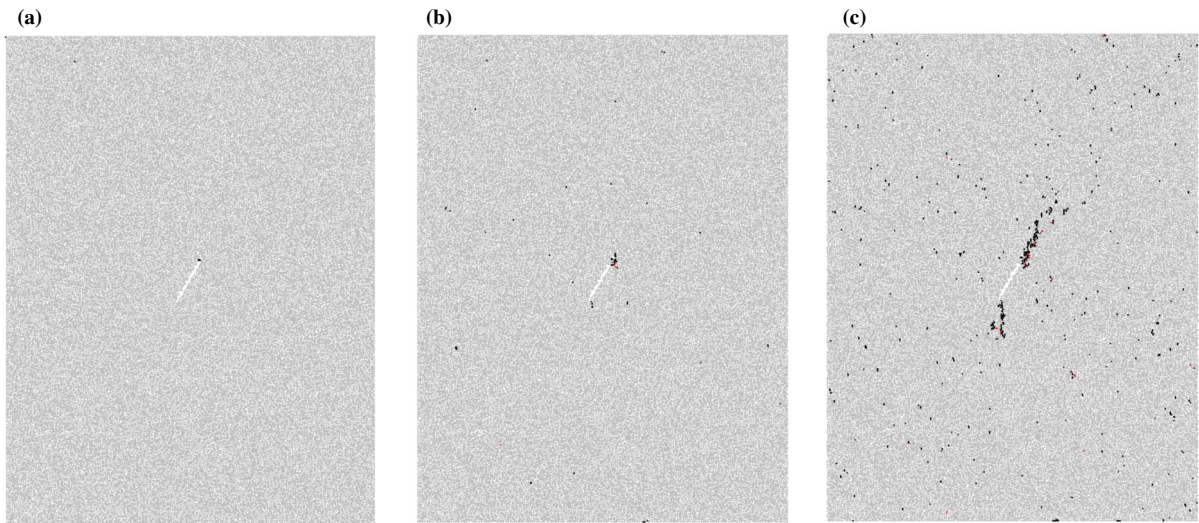


Fig. 10 Crack initiation and propagation for various axial strains: **a–c** are the crack propagation when the axial strains are 0.2, 0.3 and 0.4%

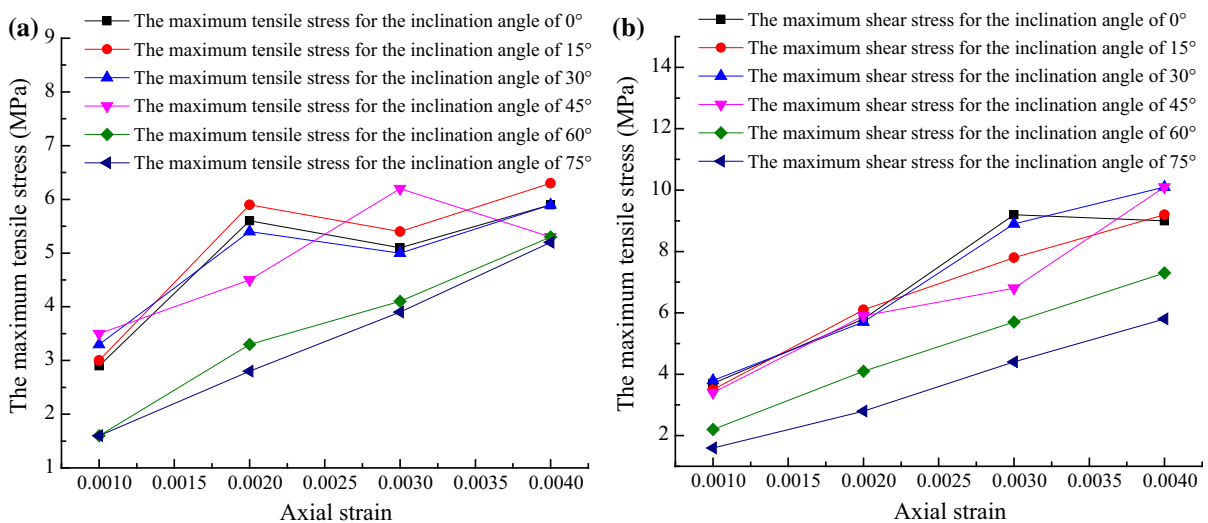


Fig. 11 The maximum tensile and shear stresses for various axial strains: **a** the maximum tensile stresses, **b** the maximum shear stress

frequently form for the axial strain that is larger than 0.3%. Thus, the shear stress concentrations before shear crack propagation might be responsible for the increase of the maximum shear stress. The increase of the maximum shear stress after shear crack propagation needs more detailed investigation.

The maximum tensile and shear stresses are shown in Fig. 12. For the axial strain of 0.1% that is lower than the wing crack initiation strain, because the increase in inclination angle from 0° to 45° will lead to the more prominent tensile stress concentrations at

prefabricated tips, the maximum tensile stress first increase and with the increase of inclination angle (Ashby and Hallam 1986). When the inclination angle is higher than 45°, the tensile stress concentration will be restrained. However, after wing crack initiation, the decreasing tensile stresses for increasing inclination angles indicate that the wing crack propagation driven by tensile stress is restrained (Fig. 12a). Simultaneously, the increase in inclination angle also restrains shear stress concentrations and need further detail investigations (Fig. 12b).

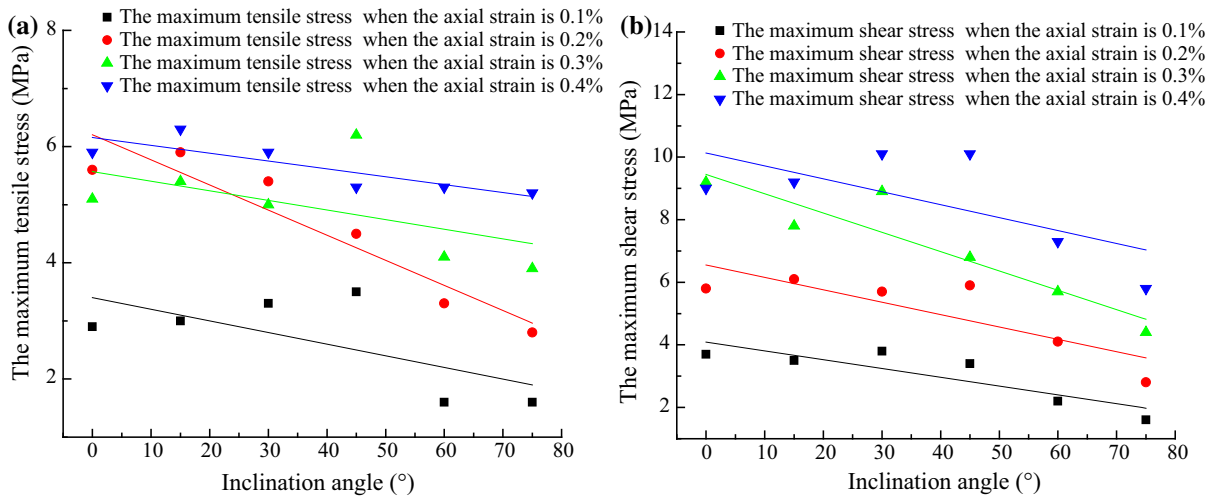


Fig. 12 The maximum tensile and shear stresses for inclination angles: **a** the maximum tensile stresses, **b** the maximum shear stress

3.3 Stress Evolution for Typical Wing and Shear Cracks

The aforementioned analysis indicates that the concentrations of the tensile stress and shear stress are responsible for the wing and secondary crack propagation. To investigate the stress evolution in the crack propagation process, as shown in Fig. 13, four monitor points (MP) were installed on the typical wing crack trajectory when the inclination angle is 0°. Simultaneously, four monitor points were installed on the

shear crack trajectory when the inclination angle is 30°.

For wing cracks, the monitored maximum principle stresses are shown in Fig. 14. The positive maximum principle stress indicates that MPs 1# and 2# are in tension in the early stage of the compression, whereas MPs 3# and 4# are compressed. The increases of the tensile stresses indicate tensile concentrations develop at these MPs. The small decrease of the tensile stress at MP 1# when the axial strain is about 0.18% may result from the micro crack formation at the left corner in Fig. 6b. When the axial strain increases to 0.25%, a sudden decrease to about 0 MPa, which is an indicator for crack propagation (Zhao et al. 2016), occurs at MPs 1#. Simultaneously, a sharp increase of the maximum principle stress at MP 2# is observed. With further increase in axial strain, the tensile stress concentration at MP 2# develops. When the axial strain reaches 0.27%, a sudden decrease followed by two sharp decrease s is observed. The first two decreases may result from the disturbance of the micro crack formation near this MP in Fig. 6c. The third sharp decrease of the maximum principle stress to about 0 MPa may result from the wing crack propagation through MP 2# in Fig. 6d. When the maximum principle stress decreases at MP 2#, a sudden jump of the maximum principle stress to about 0 MPa at MP 3# indicates that tension at MP 3# occurs. With further increase in axial strain, a similar sudden decrease of the maximum principle

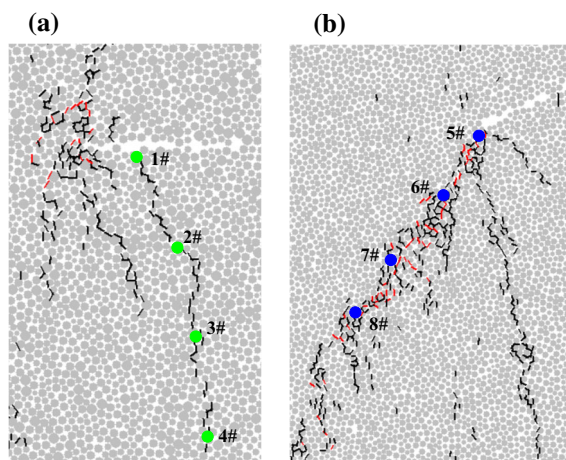


Fig. 13 Monitor points for typical wing and shear cracks: **a** monitor points for the typical wing crack when the inclination angle is 0°; **b** monitor points for the typical shear crack when the inclination angle is 30°

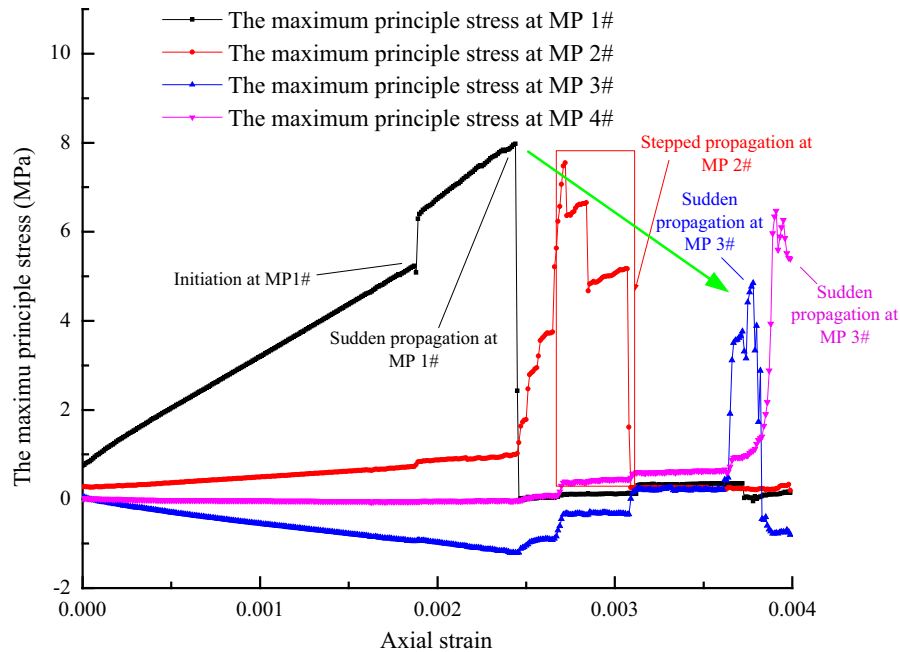
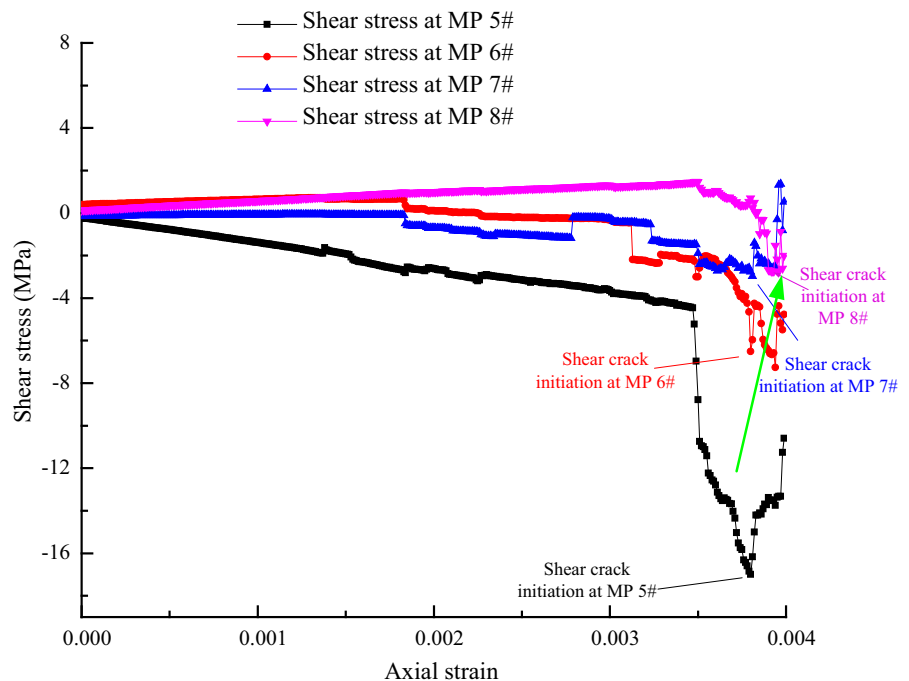


Fig. 14 The evolution of the maximum principle stress for the typical wing crack

Fig. 15 The evolution of shear stress for the shear crack



stress at MP 3# followed by a sharp increase of the maximum principle stress at MP 4# is observed. These decreases may result from the wing crack propagation through the monitor points. Whereas the

significant increases of the tensile stress at the following MP result from the transferred force.

It is interesting to note that a decrease of tensile stress with the increase in the distance between the

initiation point and the MP, which is denoted by the green arrow, is observed. A similar phenomenon was reported in Liu's study (Liu et al. 2016) where a tensile crack initiates from a circular hole. Additionally, the relatively great axial strain gap between the wing crack propagation at adjacent MP indicates that the propagation of wing crack lasts for a certain period. Thus, the tensile crack propagates in a slow and stable way.

The typical evolution of the shear stress, which drives the secondary crack initiation and propagation at MPs 5#, 6#, 7# and 8#, is shown in Fig. 15. Shear stress slowly concentrates at the tip of the prefabricated fissure (MP 5#) at the early stage of the compression. The accumulated shear stress concentration might be responsible for the increase of the maximum shear stress in Fig. 11b when the axial strain is smaller than 0.3%. When the axial strain is higher than 0.3%, shear stress concentration at MP 5# is significantly promoted. Then, a peak shear stress of about 18 MPa is observed. Then, a significant decrease of the shear stress at MP 5#, which indicates the shear stress dissipation caused by shear crack initiation, is observed. Although, shear stress significantly decreases, when the axial strain reaches 0.4%, a higher shear stress than that value for the axial strain is 0.3% is observed. Thus, the increased shear stress when the axial strain is 0.4% in Fig. 11 is properly justified. Simultaneously, this decrease causes significant increase of shear stress at MPs 6# and 7#. Then, two sudden decreases at MP 6# and 7#, which result from the shear crack propagation at these MPs, cause the significant shear stress increase at MP 8# where sudden shear stress decreases are also subsequently observed.

It can be concluded that a similar increase of the shear stress is caused by the shear stress decrease at the former MP. This increase may result from the shear stress transfer in the secondary crack propagation process. As shown in the green arrow in Fig. 14, when the distance between the MP and the initiation point of the shear crack increases, a similar decrease of the maximum shear stress for secondary crack propagation is observed. However, in the secondary crack propagation process, the axial strain gaps between the adjacent MPs for crack propagation are dramatically reduced. Thus, it can be concluded that shear cracks propagate in a more speedy and unstable way.

4 Conclusions

Stress evolution characteristics for various axial strains and inclination angles are analyzed. The results indicate that the concentration of the tensile stress is responsible for the wing crack initiation and propagation that are observed when the axial strain remains relatively low. Then, the increasing concentrated shear stress causes the initiation and propagation of the secondary crack. With the increase of the inclination angle, both tensile and shear stress concentrations tend to be restrained, and resulting in the restraint on the wing crack propagation. Additionally, in the propagation process of typical wing and secondary cracks, the sudden decreases of the tensile and shear stresses are caused by the wing and secondary crack propagation. The sudden decreases at former MP will cause the sharp increases at the latter MP, this phenomenon might result from the force transfer. Moreover, the stress evolution for typical wing and secondary cracks indicates that the wing crack tends to propagate in a steady and slow way, whereas the secondary crack propagates in a speedy and unstable way.

Acknowledgements The authors would like to acknowledge these financial supports: the China Postdoctoral Science Foundation (2017M612557), Open Fund of Hunan Provincial Key Laboratory of Safe Mining Techniques of Coal Mines (E21731), Pre-foundation for National Science foundation (YY1705) and the Youth Foundation (XJ1602) supported by Hunan Institute of Engineering.

References

- Ashby MF, Hallam SD (1986) The failure of brittle solids containing small cracks under compressive stress states. *Acta Metall* 34(3):497–510
- Bobet A, Einstein HH (1998) Fracture coalescence in rock-type materials under uniaxial and biaxial compression. *Int J Rock Mech Min Sci* 35(7):863–888
- Camones LAM, Vargas EA, Figueiredo RP, Velloso RQ (2013) Application of the discrete element method for modeling of rock crack propagation and coalescence in the step-path failure mechanism. *Eng Geol* 153:80–94
- Cao P, Liu TY, Pu CZ, Lin H (2015) Crack propagation and coalescence of brittle rock-like specimens with pre-existing cracks in compression. *Eng Geol* 187:113–121
- Cao RH, Cao P, Fan X, Xiong XG, Lin H (2016a) An experimental and numerical study on mechanical behavior of ubiquitous-joint brittle rock-like specimens under uniaxial compression. *Rock Mech Rock Eng* 49(11):4319–4338
- Cao RH, Cao P, Lin H, Pu CZ, Ou K (2016b) Mechanical behavior of brittle rock-like specimens with pre-existing

- fissures under uniaxial loading: experimental studies and particle mechanics approach. *Rock Mech Rock Eng* 49(3):763–783
- da Silva Gonçalves, Bruno Einstein HH (2013) Modeling of crack initiation, propagation and coalescence in rocks. *Int J Fract* 182:167–186
- Duriez J, Scholtès L, Donzé FV (2016) Micromechanics of wing crack propagation for different flaw properties. *Eng Fract Mech* 153:378–398
- Fan X, Kulatilake PHSW, Chen X (2015) Mechanical behavior of rock-like jointed blocks with multi-non-persistent joints under uniaxial loading: a particle mechanics approach. *Eng Geol* 190:17–32
- Gratchev I, Kim DHY, Chong K (2016) Strength of rock-like specimens with pre-existing cracks of different length and width. *Rock Mech Rock Eng* 49(11):4491–4496
- Haeri H, Shahriar K, Marji MF, Moarefvand P (2014) Experimental and numerical study of crack propagation and coalescence in pre-cracked rock-like disks. *Int J Rock Mech Min Sci* 67:20–28
- Huang D, Gu DM, Yang C, Huang RQ, Fu GY (2015) Investigation on mechanical behaviors of sandstone with two preexisting flaws under triaxial compression. *Rock Mech Rock Eng* 49(2):375–399
- Itasca CG (2002) Users' manual for particle flow code in 2 dimensions (PFC2D), Version
- Jin J, Cao P, Chen Y, Pu CZ, Mao DW, Fan X (2017) Influence of single flaw on the failure process and energy mechanics of rock-like material. *Comput Geotech* 86:150–162
- Liu T, Lin BQ, Yang W, Zou QL, Kong J, Yan FZ (2016) Cracking process and stress field evolution in specimen containing combined flaw under uniaxial compression. *Rock Mech Rock Eng* 49:3095–3113
- Wang M, Cao P (2017) Experimental study of crack growth in rock-like materials containing multiple parallel pre-existing flaws under biaxial compression. *Geotech Geol Eng*. doi:10.1007/s10706-017-0158-3
- Wong LNY, Einstein HH (2009) Systematic evaluation of cracking behavior in specimens containing single flaws under uniaxial compression. *Int J Rock Mech Min Sci* 46(2):239–249
- Xie YS, Cao P, Liu J, Dong LW (2016) Influence of crack surface friction on crack initiation and propagation: a numerical investigation based on extended finite element method. *Comput Geotech* 74:1–14
- Zhang XP, Liu QS, Wu SC, Tang XH (2015) Crack coalescence between two non-parallel flaws in rock-like material under uniaxial compression. *Eng Geol* 199:74–90
- Zhang K, Cao P, Ma GW, Wang WF, Fan WC, Li KH (2016) Strength, fragmentation and fractal properties of mixed flaws. *Acta Geotech* 11(4):901–912
- Zhao YL, Zhang LY, Wang WJ, Pu CZ, Wan W, Tang JZ (2016) Cracking and stress-strain behavior of rock-like material containing two flaws under uniaxial compression. *Rock Mech Rock Eng* 49(7):2665–2687
- Zhou XP, Cheng H, Feng YF (2013) An experimental study of crack coalescence behaviour in rock-like materials containing multiple flaws under uniaxial compression. *Rock Mech Rock Eng* 47(6):961–1986